# Supporting Information: Nanomechanics of few-layer materials: do individual layers slide upon folding?

Ronaldo J. C. Batista*[1], Rafael F. Dias[2], Ana P. M. Barboza[1], Alan B. de Oliveira[1], Taise M. Manhabosco[1], Thiago R. Gomes-Silva[1], Matheus J. S. Matos[1], Andreij C. Gadelha[3], Cassiano Rabelo[3], Luiz G. L. Cançado[3], Ado Jorio[3], Hélio Chacham[3] and Bernardo R. A. Neves[3]

Address: [1]Departamento de Física, Universidade Federal de Ouro Preto, 35400-000, Ouro Preto, MG, Brazil; [2]Departamento de Física, Universidade Federal de Viçosa, 36570-000, Viçosa, MG, Brazil and [3]Departamento de Física, Universidade Federal de Minas Gerais, 30123-970 Belo Horizonte, MG, Brazil

Email: Ronaldo J. C. Batista - batista.rjc@ufop.edu.br

* Corresponding author

The following topics are described in this supporting information.

1. Theoretical model
   (a) Deposited folded edges
   (b) Compressed folded edges
2. Sample preparation
3. SPM characterization
4. Near-field tip-enhaced Raman spectroscopy
5. Molecular dynamics simulations

# Theoretical Model

## (a) Deposited folded edges

We will consider a continuum model for the folded edges depicted in figure 2 of the main text, which shows folded edges in graphene obtained through MD simulations detailed below. We modeled such folded edge as a half tube of radius $R_0$connected to a structure we call half-soliton (two arcs of radius $r_0$[1]). Within this model, we considered that: (i) the folded edges are formed during the exfoliation process from material detached from the layered precursor, then the relevant quantity is the energy of adhesion instead of the energy of separation; (ii) We have considered the reference (zero) energy the situation where the 2D material lies straight, deposited on a substrate. Thus, can write the energy to form folded edges as composed of two terms:

- $E_{adhesion} = \alpha L(\pi R_0 + 2\theta_0 r_0)$, which accounts for the energy cost to detach from a precursor layered material, the amount of 2D material required to form the folded edge, i. e., ribbons of length $L$ whose widths are $\pi R_0$ e $2\theta_0 r_0$, respectively.

- $E_{bending} = \int \frac{\kappa ds}{R_0^2} + 2\int \frac{\kappa ds'}{r_0^2} = L\frac{\kappa}{2}(\frac{\pi}{R_0} + \frac{2\theta}{r_0})$, which refers to the energy necessary to bend ribbons of length $L$ and widths $\pi R_0$ and $2\theta r_0$ in the form or arc circles.

$\alpha$ is the adhesion energy per unit area between layers of the 2D material, and $\kappa$ is the bending stiffness of the 2D material. Then, energy to form the folded edge per unit of length is:

$$\varepsilon = \frac{E_{adhesion} + E_{bending}}{L} = \alpha(\pi R_0 + 2\theta_0 r_0) + \frac{\kappa}{2}\left(\frac{\pi}{R_0} + \frac{2\theta}{r_0}\right). \tag{1}$$

$\varepsilon$ is a function of the variables $R_0$, $r_0$ and $\theta_0$, which are all related through the expression: $2R_0 - d = 2r_0(1 - \cos\theta_0) \approx r_0\theta^2$, see figure 2 of the main text. Minimizing $\varepsilon$ subject to the constraint $g = 2R_0 - d - r_0\theta^2$, we obtain:

$$r_0 = \sqrt{\frac{3\kappa}{2\alpha}} \tag{2}$$

and

$$3\pi - \frac{{r_0}^2\pi}{R_0^2} + \frac{8\sqrt{r_0}}{\sqrt{2R_0 - d}} = 0. \tag{3}$$

## (b) Compressed folded edge

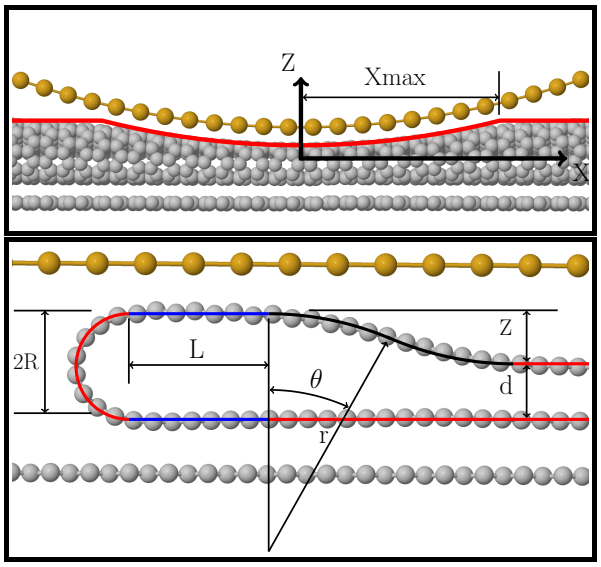


**Figure 1:** Molecular dynamics simulations of a folded edge in graphene (gray circles) deposited on a graphene substrate compressed by a hard cylinder of radius 10 nm (yellow circles) **Top panel**: front view of the compressed folded edge. **Bottom panel**: a cross section of the folded edge shown in the top panel. The red, blue and black lines show our model for the cross section geometry of the compressed folded edge.

In this section, we considered that a spherical probe of radius $R_s$ compresses the folded edge described in the previous section. To obtain an analytical expression for the force as a function of the deformation caused by the probe tip, we applied the following assumptions:

- folded edges compressed by spherical probes have cross-section geometries similar to that described by the red, blue and black lines of the bottom panel of figure 1, which also shows the geometry of compressed graphene folded edge obtained through MD simulations.

- The reference (zero) energy is the situation where the 2D material lies straight, deposited on

another layer of the same 2D material, as shown in figure 1 of the main text for talc folded edges.

- The relevant quantities are the energies of adhesion per unit of the area between layers ($\alpha$) and between layer and probe ($\alpha_p$) instead of the energy of separation.

Figure 1 shows that the curved parts of the folded edge are still very well described by a half tube and a half-soliton model. However, a flat region of width $l$ appears between them, demanding an additional energetic contribution in Eq. 1. Because the region $l$ is contact with the probe, its contribution the energy is $(\alpha - \alpha_p)l$. Thus, the energy per unit of length of a compressed folded edge is the sum of adhesion and binding energies as follows:

$$\varepsilon = (\alpha - \alpha_p)l + \alpha(\pi R + 2\theta_0 r) + \frac{\kappa}{2}\left(\frac{\pi}{R} + \frac{2\theta}{r}\right). \tag{4}$$

The compression applied by the probe deposits the half-soliton on the probe itself. Because the half-soliton length ($2r_0\theta_0$) exceeds its horizontal projection ($2r_0 sin\theta_0$), the difference $2r_0(\theta_0 - sin\theta_0) - 2r(\theta - sin\theta)$ contributes to the size of blue flat regions of the figure 1. Another contribution, $\pi(R_0 - R)$, comes from the reduction of the half tube diameter relative to its uncompressed value ($R_0$). Thus, $2l = \pi(R_0 - R) + 2r_0(\theta_0 - sin\theta_0) - 2r(\theta - sin\theta)$ and energy can be rewritten as follows:

$$\varepsilon = (\alpha - \alpha_p)\left[\frac{\pi}{2}(R_0 - R) + r_0(\theta_0 - sin\theta_0) - r(\theta - sin\theta)\right] + \alpha\pi R + \frac{\kappa\pi}{2R} + 2\theta\left(\alpha r + \frac{\kappa}{2r}\right). \tag{5}$$

Minimizing $\varepsilon$ subjected to the constraint: $g = 2R - d - r\theta^2$, we obtain: $r \approx r_0 = \sqrt{\frac{3\kappa}{2\alpha}}$ (We considered $-\frac{(\alpha-\alpha_p)\theta^2}{12} + \alpha \approx \alpha$, which is reasonable because $(\alpha - \alpha_p)$ should be significantly smaller than $\alpha$, and because $d > R_0$ for all foldeds, $\frac{\theta^2}{12} < \frac{R_0}{12r_0} = \frac{1}{12\sqrt{3}}$). Using $\kappa = \frac{2r_0^2\alpha}{3}$ and $sin\theta \approx \theta - \frac{\theta^3}{3!}$ we obtain:

$$\varepsilon = (\alpha - \alpha_p)\left[\frac{\pi}{2}R_0 + r_0(\theta_0 - sin\theta_0) - r_0\frac{\theta^3}{6}\right] + (\alpha + \alpha_p)\frac{\pi}{2}R + \frac{r_0^2\pi\alpha}{3R} + \frac{8\alpha\theta r_0}{3}. \quad (6)$$

Defining $z = 2R - d$ and using $2R - d = 2r_0(1 - \cos\theta_0) \approx r\theta^2$ to eliminate $\theta$ ($\theta = -\sqrt{z/r_0}$), the above equation can be rewritten as follows:

$$\varepsilon = (\alpha-\alpha_p)[\frac{\pi}{2}R_0+r_0(\theta_0-sin\theta_0)+\frac{z^{3/2}}{6\sqrt{r_0}}]+(\alpha+\alpha_p)\frac{\pi}{2}\frac{(z+d)}{2}+\frac{2r_0^2\pi\alpha}{3(z+d)}-\frac{8\alpha\sqrt{z}\sqrt{r_0}}{3}. \quad (7)$$

We can write the force per unit length that the folded applies on the probe as a function of $z$ as follows:

$$f(z) = -\frac{dE}{dz} = (\alpha_p - \alpha)\frac{\sqrt{z}}{4\sqrt{r_0}} - (\alpha + \alpha_p)\frac{\pi}{4} + \frac{2r_0^2\pi\alpha}{3(z+d)^2} + \frac{4\alpha\sqrt{r_0}}{3\sqrt{z}}. \quad (8)$$

From Eq. (8), the force applied in a 3D probe by the folded edge can be obtained, provided that the probe profile over the folded length is known. Let us define such a direction as $x$, as shown in the upper panel of figure 1. From here we can write

$$F(h) = \int_{x_{\min}}^{x_{\max}} f(x)dx, \quad (9)$$

where $f(x)$ is force per unit length and $h$ is a parameter that determines the probe height. For an object whose profile over the folded length is an arc circle (see the top panel of figure 1), Eq. 9 becomes:

$$F(h) = 2\int_{0}^{x_{\max}} f(x)dx = 2\int_{h}^{2R_0-d} f(z)\frac{dx}{dz}dz =$$

$$2\int_{h}^{2R_0-d} f(z)\frac{z-(R_s-h)}{\sqrt{R_s^2-(z-R_s-h)^2}}dz, \tag{10}$$

where $R_s$ is the probe radius and $h$ and $2R_0 - d$ are the minimal and maximal values of variable $z$, respectively. Eq. 10 can be rewritten as follows:

$$F(h) = 2\int_{h}^{2R_0-d} f(z)\frac{dz}{\sqrt{\frac{R_s^2}{(z-R_s-h)^2}-1}} =$$

$$2\int_{h}^{2R_0-d} f(z)\frac{dz}{\sqrt{(1+\frac{z-h}{R_s}+(\frac{z-h}{R_s})^2+...)^2-1}}$$

$$\approx 2\sqrt{\frac{R_s}{2}}\int_{h}^{2R_0-d}\frac{f(z)dz}{\sqrt{z-h}}, \tag{11}$$

where terms of the order $[(z-h)/R_s]^2$ and superior are neglected because $z - h$ at most equals to deformations caused by the probe ($D = 2R_0 - d - h$), which are usually significantly smaller than $R_s$. Inserting Eq. (8) in Eq. (11) and solving the integrals we obtain:

$$F(D) = \sqrt{2R_s}\left[\frac{-(\alpha+\alpha_p)\pi}{2}\sqrt{D} + \frac{2r_0^2\pi\alpha}{3}\left(\frac{atan\sqrt{\frac{D}{2R_0-D}}}{(2R_0-D)^{3/2}} + \frac{\sqrt{D}}{(2R_0-D)2R_0}\right)\right.$$
$$\left.+\left(\frac{(\alpha_p-\alpha)(2R_0-d-D)}{8\sqrt{r_0}} + \frac{4\alpha\sqrt{r_0}}{3}\right)ln\left(\frac{\sqrt{2R_0-d}+\sqrt{D}}{\sqrt{2R_0-d}-\sqrt{D}}\right) + \frac{(\alpha_p-\alpha)}{4\sqrt{r_0}}\sqrt{2R_0-d}\sqrt{D}\right] \tag{12}$$

$R_0$ and $d$ can be determined from AFM height profiles and $r_0$ can be determined from Eq. (3).

Also, $R_s$ is usually known in AFM experiments, which leaves two adjustable parameters in Eq. (12): $\alpha$ and $\alpha_p$.

The force the compressed folded edge applies on the probe can be written as a function of the strain ( $S = \frac{D}{2R_0 - d}$) as follows:

$$\begin{aligned}\frac{F(S)}{\sqrt{2R_s}\sqrt{r_0}} &= \frac{-(\alpha+\alpha_p)\pi}{2}\sqrt{\frac{2R_0-d}{r_0}}\sqrt{S} + \frac{(\alpha-\alpha_p)}{4}\frac{2R_0-d}{r_0}\sqrt{S} \\ &+\frac{2\pi\alpha}{3}\left(\frac{r_0}{2R_0}\right)^2\sqrt{\frac{2R_0-d}{r_0}}\left(2\sqrt{S} + \frac{8}{3}\left(1-\frac{d}{2R_0}\right)^{3/2}S^{3/2} + 3\left(1-\frac{d}{2R_0}\right)^{5/2}S^{5/2}\right) \\ &+\left(\frac{(\alpha_p-\alpha)(1-S)}{8}\frac{2R_0-d}{r_0} + \frac{4\alpha}{3}\right)ln\left(\frac{1+\sqrt{S}}{1-\sqrt{S}}\right),\end{aligned} \tag{13}$$

where we use $atan\left(\sqrt{\frac{D}{2R_0-D}}\right) \approx \sqrt{\frac{D}{2R_0-D}} - \frac{1}{3}\left(\frac{D}{2R_0-D}\right)^{3/2}$ and neglected terms of the order $(D/2R_0)^3$ and superior in the expansion of $\frac{1}{1-D/2R_0}$. We also divided both sides of the above equation by $\sqrt{r_0}$. If the folded edges have the same proportions, that is, the same values of $\frac{r_0}{R_0}$ and $\frac{d}{r_0}$, a graph of $\frac{F(S)}{\sqrt{2R_s}\sqrt{r_0}}$ vs strain will be similar for folded edges of different thickness. In fact, the bottom panel of figure 4 of the main text shows that talc folds of thickness varying from 1 up to 11 nm present similar dependence of $\frac{F(S)}{\sqrt{2R_s}\sqrt{r_0}}$ with strain.

# Materials and Methods

## Sample Preparation

The graphene and talc samples were prepared by the mechanical exfoliation onto a 300nm-thick Si oxide layer covering the Si substrate. folded layers were initially identified using optical microscopy and, then, scanned by AFM.

## SPM characterization

In all results shown in this paper, NSC18/NoAl silicon cantilevers with typical spring constant k ≈2.8 N/m, nominal radius of curvature r≈10 nm and resonant frequency $\omega_0$ ≈ 75 kHz was em-

[] 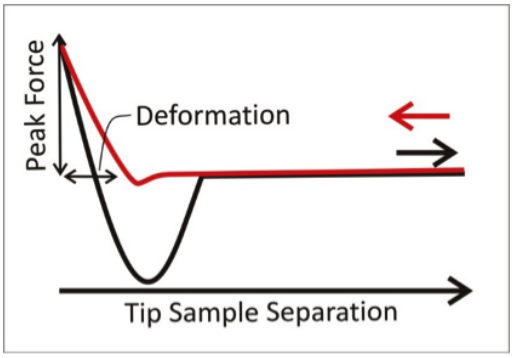


**Figure 2:** Schematic plot force versus tip-sample distance and the deformation value.

ployed. More accurate estimations of k and r were carried out by the use of the Sader's method[4] and by imaging reference samples, respectively. The AFM characterization was carried out on a Bruker MultiMode SPM using the Peak Force Quantitative Nano-Mechanical imaging mode®[5]. With the Peak Force QNM imaging mode® we can measure the maximum deformation of the sample, defined as the penetration of the tip into the surface at the Peak Force (highest force). As the load on the sample under the tip increases, the deformation also increases. The measured deformation may include both elastic and plastic contributions. We work in the elastic regime. Maximum sample deformation is calculated from the difference in separation from the point where the force is zero to the peak force point along the approach curve (see Fig. 2).[5] The hysteresis loop in Fig. 2 is related to the dissipated energy during the PeakForce loop (tip approach and retraction).[5]

## Near-field tip-enhanced Raman spectroscopy

For TERS measurements, we use a radially polarized laser beam with a 633 nm (1.96 eV) excitation energy and a home-built AFM scan-head, working in a shear-force mode. The optical and AFM systems are coupled via a gold plasmon-tuned tip pyramids (PTTP)39[6], to get the tip-enhanced Raman signal. We use a laser power of 100 $\mu$W to avoid sample heating.

## Molecular Dynamics Simulations

We performed molecular dynamics simulations using the LAMMPS package[7]. Our system is composed of a graphene folded on a graphene layer the two of them containing 6804 atoms. The

graphene layer was kept "frozen" during all simulations, i.e., the resultant force on every atom of this layer was set to zero. Carbon atoms were modeled classically using the adaptive intermolecular reactive empirical bond order (AIREBO) potential for the C-C interaction[8]. Periodic boundary condition was used in the y and x direction, see Fig. 1, while z was finite. To model the AFM tip we use a cylinder composed of 672 Lennard-Jones particles, which were not allowed to move relative to each other. The Lennard-Jones parameters for the AFM-C interaction were $\varepsilon$=1 meV and $\sigma$=3 Å. Simulations were performed in the canonical ensemble. The Nosé-Hoover thermostat[9,10] was used in order to keep the temperature T = 300 K. The timestep used was 0.001 ps.

# References


1. de Lima, A. L.; Muessnich, L. A. M.; Manhabosco, T. M.; Chacham, H.; Batista, R. J. C.; de Oliveira, A. B. *Nanotechnology* **2015**, *26* (4), 045707–045714.

2. Girifalco, L. A.; Lad, R. A. *The Journal of Chemical Physics* **1956**, *25* (4), 693–697.

3. Barboza, A. P. M.; Chacham, H.; Neves, B. R. A. *Phys. Rev. Lett.* **2009**, *102*, 025501.

4. Sader, J. E.; Chon, J. W. M.; Mulvaney, P. *Review of Scientific Instruments* **1999**, *70* (10), 3967–3969.

5. Sahin, O.; Erina, N. *Nanotechnology* **2008**, *19* (44), 445717.

6. Vasconcelos, T. L.; Archanjo, B. S.; Oliveira, B. S.; Valaski, R.; Cordeiro, R. C.; Medeiros, H. G.; Rabelo, C.; Ribeiro, A.; Ercius, P.; Achete, C. A.; Jorio, A.; Cançado, L. G. *Advanced Optical Materials* **2018**, *6* (20), 1800528.

7. Plimpton, S. *Journal of Computational Physics* **1995**, *117* (1), 1 –19.

8. Stuart, S. J.; Tutein, A. B.; Harrison, J. A. *The Journal of Chemical Physics* **2000**, *112* (14), 6472–6486.

161 9. Nosé, S. *The Journal of Chemical Physics* **1984**, *81* (1), 511–519.

162 10. Hoover, W. G. *Phys. Rev. A* **1985**, *31*, 1695–1697.